Atomic Scale Control of Spin Current Transmission at Interfaces

Mohamed Amine Wahada,* Ersoy Şaşıoğlu, Wolfgang Hoppe, Xilin Zhou, Hakan Deniz, Reza Rouzegar, Tobias Kampfrath, Ingrid Mertig, Stuart S. P. Parkin, and Georg Woltersdorf*

Cite This: *Nano Lett.* 2022, 22, 3539−3544

Read Online

ACCESS | Metrics & More | Article Recommendations | SI Supporting Information

ABSTRACT: Ferromagnet/heavy metal bilayers represent a central building block for spintronic devices where the magnetization of the ferromagnet can be controlled by spin currents generated in the heavy metal. The efficiency of spin current generation is paramount. Equally important is the efficient transfer of this spin current across the ferromagnet/heavy metal interface. Here, we show theoretically and experimentally that for Ta as heavy metal the interface only partially transmits the spin current while this effect is absent when Pt is used as heavy metal. This is due to magnetic moment reduction at the interface caused by 3d−5d hybridization effects. We show that this effect can be avoided by atomically thin interlayers. On the basis of our theoretical model we conclude that this is a general effect and occurs for all 5d metals with less than half-filled 5d shell.

KEYWORDS: *Ultrafast demagnetization, Ultrafast spin current, THz currents, Orbital hybridization, Spin pumping, Spin Hall effect*
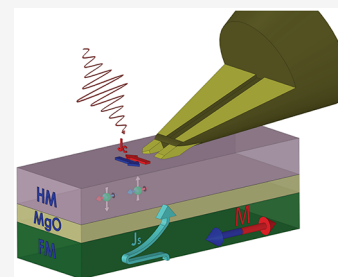
Spin current (SC) is the net flow of angular momentum and in condensed matter usually carried by the spin degree of freedom of electrons.[1] The discovery that the magnetization vector can be controlled in nanostuctures using spin currents[2−5] has generated enormous interest in the field of spintronics. This effect is essential for spin-based nonvolatile memory applications, displacement of spin textures such as chiral domain walls and skyrmions for racetrack applications,[6−10] or spin torque oscillators.[11]

A spin-polarized current may be produced electrically by passing a current through a ferromagnet (FM). Alternatively, an unpolarized charge current can be used to generate spin polarization at the surface of a nonmagnetic heavy metal (HM) with spin−orbit coupling (SOC) via the spin Hall effect (SHE).[12−14] The efficiency of this conversion is material-dependent and usually quantified by the spin Hall angle. When interfaced with a FM, the spin current is transmitted through the interface and can exert a torque on the magnetization, a phenomenon known as spin orbit torque (SOT). Reciprocally, spins can be pumped from the FM into the HM where the SC is converted to a charge current via the inverse SHE (ISHE). This approach may be demonstrated via microwave-induced precession of the magnetization[13,15] or via ultrafast optical excitation.[16,17] The latter example is the basis of ultrabroadband and efficient terahertz (THz) emitters.[17−19]

The key element for these processes is the FM/HM interface.[20] Mainly, two effects can impair the spin-current transmission: (i) the magnitude of the spin-mixing conductance[21] and (ii) spin-memory loss (SML).[22−25] SML has first been considered in magnetoresistance experiments.[26,27] The possible underlying mechanisms for SML are still debated. Nevertheless, it is believed to be related to interface spin−orbit coupling (i-SOC),[25,28−31] noncollinear magnetization, disor-

der,[22,32] and lattice mismatch.[22] SML due to i-SOC is often evoked in order to explain inconsistencies of the value of the spin Hall angle in spin transport experiments.[33−36]

Separating, understanding, and finally controlling these interface properties is an essential step to enhance the spin-current injection efficiency. Up to now, only a limited number of studies have been performed in regard of this complex problem,[20,37−46] using, for example, interface alloying and interlayer insertion. For the giant magnetoresistance samples, the insertion of interface dusting layers leads to a dramatic enhancement of the magnetoresistance.[47,48] In the same spirit, using nonmagnetic dusting layers between FM and HM allows one to increase the efficiency of current-induced chiral domain-wall motion.[49]

In this work, we use MgO as an interlayer with varying thicknesses placed at the HM/FM interface. To identify the SML processes, two experiments are used to independently determine (i) the total amount of spin current injected by the ferromagnet and (ii) the amount of spin current delivered into to the HM. By performing optical ultrafast spin injection and ISHE charge current detection, we demonstrate that ultrathin MgO layers reduce the spin-current transmission differently depending on the HM element. While we find a reduction for HM = Pt, it is rather enhanced for HM = Ta. On the basis of electronic and transport calculations, we link this effect to the magnetic
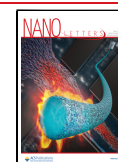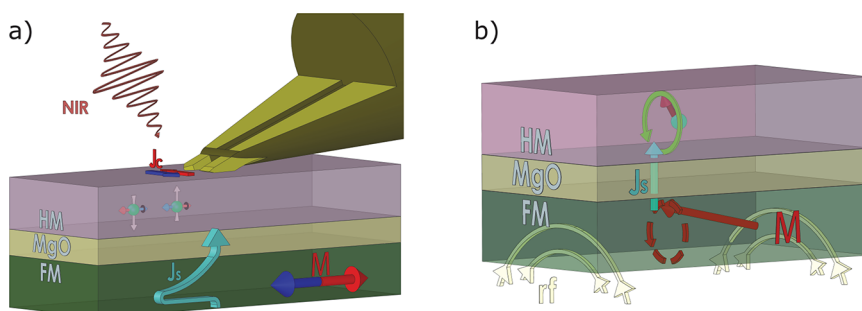
Figure 1. Experimental configuration. (a) Ultrafast measurement of the ISHE using optical excitation and electronic detection. A pulsed femtosecond laser excites the HM/FM bilayer and creates an ultrafast spin current pulse J_s propagating across the MgO interlayer into the HM where it is converted into a charge current J_c picked up by a rf-probe tip. (b) In a complementary spin pumping experiment, a continuous rf field excites the magnetization, causing its precession, which generates a spin current that is pumped from FM to HM. The spin transport into the HM enhances the damping in the FM.
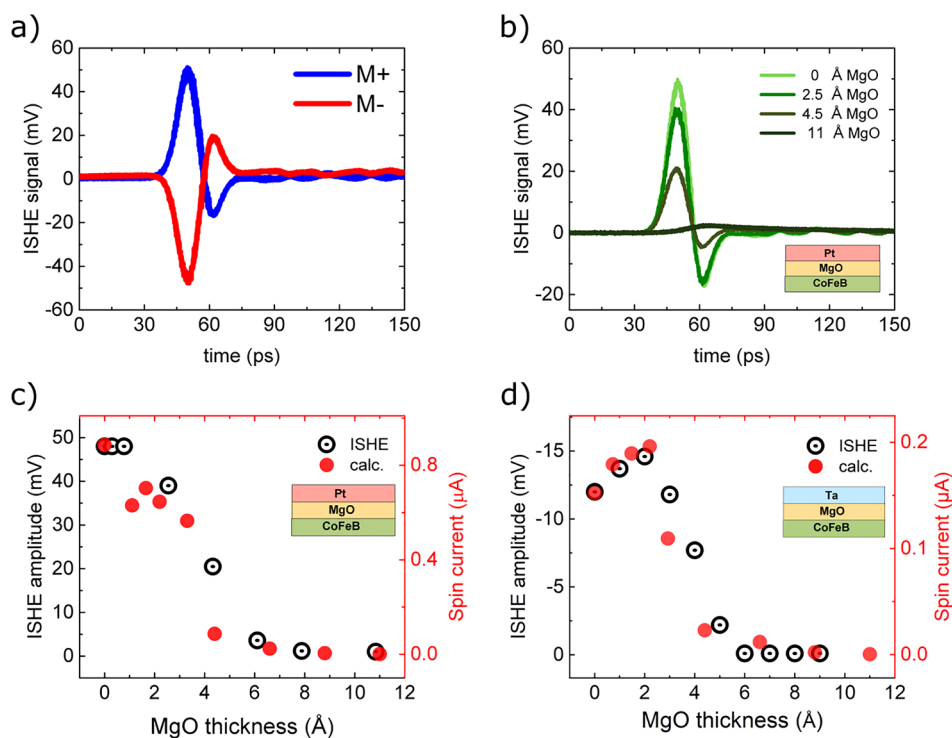

Figure 2. Ultrafast ISHE measurements. (a) Time-resolved ISHE signal for opposite magnetization directions. (b) Time-resolved ISHE signal for HM = Pt sample with different MgO thicknesses ranging from 0 to 17 Å. (c,d) MgO-thickness dependence of the ISHE signal amplitude and the calculated spin-current transmission per unit cell for HM = Pt and HM = Ta, respectively. Note that for HM = Ta, the ISHE signal has negative values due to the negative sign of the spin Hall angle of Ta.

moment reduction at the FM/Ta interface. By the additional measurement of the total spin momentum pumped by the FM across the interface (spin pumping), we estimate the magnitude of SML. We conclude that SML is not a significant effect for the interfaces investigated here.

■ RESULTS AND DISCUSSION

Ultrafast spin current pulses are generated by exciting the layer stack with optical femtosecond laser pulses. The ISHE converts these spin current pulses into charge currents, which are typically detected in the form of free-space THz radiation using electro-optic sampling.[17] Here, we use a coplanar probe tip to detect the sub-THz current pulse directly on the sample as shown in Figure 1a. Typical results are shown in Figure 2a.

As a next step, we examine the influence of ultrathin MgO interlayers on the inverse SHE signals for HM = Pt. Different

waveforms are shown in Figure 2b for various MgO thicknesses. The amplitudes of the signals are displayed in Figure 2c. As a function of the MgO thickness, one observes a plateau-like behavior for up to 2 Å of the MgO layer corresponding to the thickness of a MgO unit cell. For a larger thickness, the signal decays exponentially with a decay length of 2 Å. Next, these experiments are repeated for HM = Ta. The results in Figure 2d surprisingly show an increase of the signal of more than 20% for small thicknesses of MgO (up to 2 Å). For larger thicknesses, again an exponential decay with a similar characteristic length scale as for HM = Pt is observed. We note that the signal amplitude vs MgO thickness exhibits identical behavior when we employ broadband free-space THz field detection (see Figure S3).

To reveal the mechanism responsible for the enhanced ISHE signal in samples with a MgO interlayer and HM = Ta, ab initio
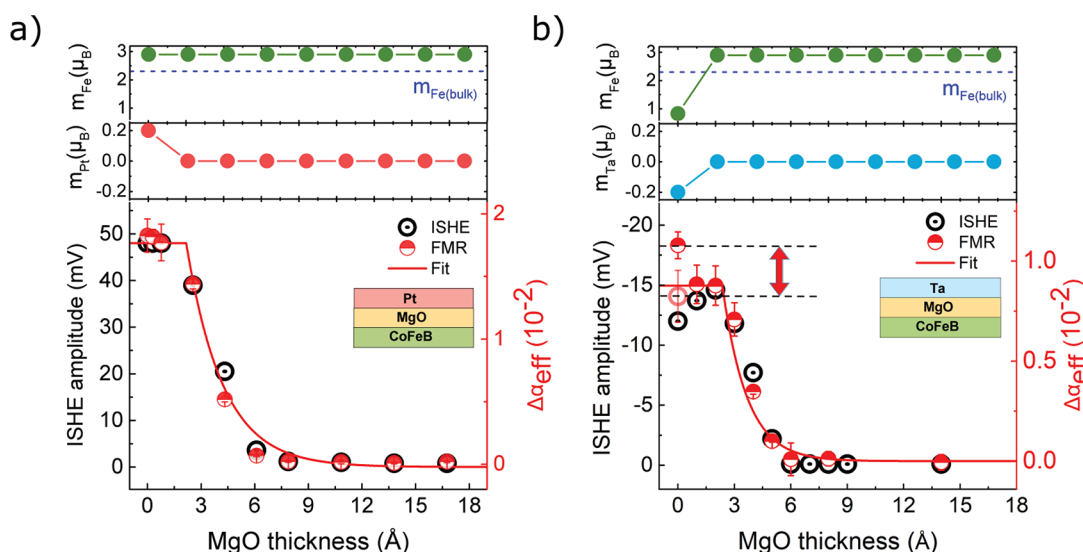
Figure 3. ISHE signals, enhanced damping, and interface magnetic moments. MgO-thickness dependence of the ISHE signal amplitude and the enhanced damping due to spin pumping for (a) HM = Pt and (b) HM = Ta. The top panels of (a,b) show the calculated magnetic moment per atom at the interface for (a) Fe and Pt and (b) Fe and Ta. The red open circle in panel (b) represents the corrected enhanced damping by considering the reduced magnetic moment as determined by the VSM measurement. The red fit is a plateau up to 2.2 ± 0.1 Å followed by an exponential decay with a decay length of 2 ± 0.2 Å.

transport calculations are combined with density-functional theory (DFT) calculations. To model the laser-excited electronic transport, we use a Landauer-Buettiker approach with a bias voltage of 50 mV. We justify this approach based on the fact that hot electrons thermalize within around 100 fs to a Fermi−Dirac-type distribution whose edge covers a ∼50 meV wide energy window around the Fermi level. Figure 2c,d shows the calculated MgO thickness dependence of the SC. To compare the experiment with the calculations, we scale the two data sets at zero MgO thickness. Clearly, for both HM = Pt and HM = Ta, the calculated SC reproduces well the corresponding experimental ISHE data. For the case of Pt, the spin current decreases monotonically with the MgO thickness after showing a plateau behavior up to 2 Å. By contrast, when Ta is used as HM, one first finds an increase of the SC up to 1 monolayer (ML) of MgO followed by a rapid decay matching well the experimental results.

To understand the origin of the overall rapid decay of the SC with increasing MgO thickness, we consider the projected local density of states (LDOS) for both systems, where the thickness t of MgO barrier varies from 1 to 4 ML. As seen in Figures S8 and S9, the MgO layer is actually metallic for a thickness of up to 2 ML and only starts opening a band gap for thicknesses larger than 3 ML. With increasing MgO barrier thickness, the transport mechanism changes gradually from a metallic transport to a tunneling behavior and, as expected the SC drops exponentially with a decay length of 2 Å as shown in Figure 2c,d.

Figure S6b shows the spin- and energy-dependent transmission spectrum for the case of Fe/Ta and Fe/MgO(1 ML)/Ta. The corresponding k-dependent transmissions are presented in Figures S10 and S11. One finds that, around the Fermi level, the transmission is reduced by more than 50% for both spin channels when 1 ML of MgO is inserted at the Fe/Ta interface. However, this reduction is larger for the spin-down channel (minority-spin), which leads to an enhancement of the overall SC. In other words, the absolute value of the transmission difference $T^{\uparrow} - T^{\downarrow}$ at the Fermi level for Fe/MgO(1 ML)/Ta is about 30% larger than the corresponding value in the Fe/Ta case

(see Figure S6b). This enhancement of the SC (see Figure 2d) is linked to the recovery of the magnetic moment of Fe (or Co) and thus the spin polarization at the Fe/Ta (CoFeB/Ta) interface.

It is known that when elementary 3d ferromagnets are interfaced with transition metals with less than a half-filled 5d shell such as Hf, Ta, or W, the magnetic moment at the interface is reduced.[50] In some cases (e.g., $Ni_{81}Fe_{19}$), this effect can even give rise to the formation of a magnetically dead layer.[51] The suppression of the magnetic moment can be qualitatively explained on the basis of the Stoner model by considering the density of states $N(E_F)$ at the Fermi level (see Figures S12 and S14a) and the Stoner parameter (see Section S2 in Supporting Information). Because of extended 5d orbitals of the early transition metals, the strong Fe(3d)−Ta(5d) hybridization at the interface transfers the Fe-3d weight around the Fermi level to lower energies. Therefore, $N(E_F)$ is substantially reduced, and the Stoner criterion for the Fe atoms at the interface is hardly satisfied. Note that for simplicity, only Fe atoms are considered in the calculations. However, we wish to point out that for Co atoms at the interface, the reduction of $N(E_F)$ is even larger than for the Fe case as illustrated in Figures S13 and S14b. Thus, the Co magnetic moments at the interface with Ta are also strongly suppressed. As one moves from the left to the right within the row of elements in the periodic table, the nuclear charge of the HM increases, causing the d-wave functions to contract. This effect reduces the hybridization between Fe(3d)−Pt(5d) orbitals and causes an enhancement of the Fe magnetic moments at the Fe/Pt interface.

The DFT-calculated values of interface magnetic moments are presented in Table S1 and show that the spin magnetic moment of the Fe atoms at the interface layer are reduced to an average value of $0.8 \mu_B$, which only corresponds to 30% of the Fe bulk magnetic moment. The reduced spin polarization at the interface layer also leads to a reduced spin-current transmission. Interestingly, the insertion of 1 ML MgO at Fe/Ta junction causes the recovery of magnetic moment of Fe at the interface,

resulting in an enhancement of the spin-dependent transmission and SC in agreement with experimental data.

To better understand the MgO interlayer dependence of the ISHE signal for HM = Ta layers, we now consider the total spin current pumped out of the FM layer. For this purpose, we use the ferromagnetic resonance (FMR) technique (see Figure 1b and Methods in Supporting Information) and measure the additional damping caused by the MgO/HM capping layers due to spin pumping as shown in Figure S17. This effect is sensitive to the total spin current emitted by the ferromagnet,[52] while the electrically measured ISHE signal is only sensitive to the fraction of the spin current pumped into the HM layer, as illustrated in Figure 1. We emphasize here that, despite the difference in the excitation energies between the two techniques, the relevant electronic transport occurs in a small energy window close to the Fermi level. It has been recently demonstrated that ultrafast laser excitation leads to a generalized spin voltage driving the spin current.[53] This notion is supported by measurements where the spin current does not depend on the photon energy from 0.8 to 1.5 eV.[54] Here, we extend this range by showing results between 1.1 and 4.4 eV (Figure S7). We find no notable difference of the ISHE signal for the three different photon energies as a function of the MgO barrier thickness.

In Figure 3, we show the enhanced damping $\Delta\alpha$ due to the proximity of the HM layer as a function of the MgO interlayer thickness and compare it to the thickness dependence of the corresponding ISHE signal. For the case of HM = Pt, the ISHE signal and the additional damping exhibit the same MgO-thickness dependence as shown in Figure 3a. This implies that the spin current that is generated in the FM is fully delivered to the Pt layer. In contrast, for HM = Ta, the ISHE signal and the additional damping diverge for small MgO interlayers, as shown in Figure 3b. Enhanced damping and ISHE signals match well for MgO thicknesses ≥2 Å. For zero MgO thickness (i.e., the direct CoFeB/Ta interface), they deviate by about 30%. At first glance, this implies that part of the spin current pumped in the HM = Ta case is not delivered to the HM layer and lost at the interface. However, one needs to consider the magnetic moment suppression at the FM/Ta interface. From the calculations (which correspond to zero temperature) one expects only one atomic layer with reduced magnetization. At 300 K, thermal fluctuations enhance the thickness range of the suppressed moment to about three atomic layers. This effect is often referred to as magnetically dead interface layer[55−58] and was confirmed for the present samples using vibrating sample magnetometry (VSM) as shown in Figure S15. For a 2 nm thick CoFeB layer, the depolarization of three atomic layers corresponds to a reduction of the magnetic moment by about 25%. Since the enhanced damping scales inversely with the magnetic moment per interface area as $1/(M_s d)$, where d is the thickness of the magnetic layer,[52,59] one can expect an increase of the enhanced damping by 25% when the MgO spacer layer is absent. Hence, most of the deviation between enhanced damping and ISHE amplitudes can be explained by this effect.

In the following, we discuss the relevance of spin memory loss (SML) for the experiments above. SML can be quantified by the parameter δ as follows

$$J_s^{HM} = (1 - \delta)J_s \qquad (1)$$

Here, J_s^{HM} is the spin current on the HM side, and J_s is the total spin current pumped from the FM side. In the case of HM = Pt, there is very close correspondence between the ISHE voltage

and the enhanced damping due to spin pumping implying that SML is a small effect at the Pt/CoFeB interface with $\delta_{Pt} \leq 0.05$. For HM = Ta, the results imply that $\delta_{Ta} \leq 0.10$ is needed to account for the remaining difference between enhanced damping and ISHE signals. With the insertion of 1 ML of MgO, the magnetic moment recovery at the interface enhances the spin current transmission and simultaneously suppresses the enhanced damping as well as the SML (see Figure 3b).

We want to point out that SOC is neglected in the transport calculations. To estimate the impact of SOC at the various interfaces, we calculate the layer-resolved magnetic anisotropy energy (MAE) (see Figure S16). At the Fe/Ta interface, MAE is enhanced by more than a factor of 5 compared to the Fe/Pt or the Fe/MgO interface. This is in line with the experiments indicating enhanced spin relaxation for the FM/Ta interface.

Inserting MgO interlayers between FM and HM layers suppresses the spin current transmission exponentially with a decay length of ∼2 Å. This effect can be well explained by the calculated spin-current transmission. By combining ISHE and spin-pumping measurements as a function of MgO thickness, we demonstrate a connection between reduced magnetic moments at the HM/FM interface and potentially a small SML contribution at the CoFeB/Ta interface. On the basis of calculations of the electronic structure, we conjecture that the effect of interface moment reduction occurs for all 5d heavy metals with less than half-filled d-shells[50] when interfaced with 3d ferromagnets. The insertion of an atomically thin MgO interlayer is sufficient to recover the interface spin polarization of the ferromagnet. We demonstrated that spin current transmission for two highly relevant HM/FM interfaces can be modeled well without considering spin relaxation (such as SML). Hence, we conclude that it is physically more reasonable to discuss the incomplete spin current transmission across these interfaces by a transmissivity parameter (related to the matching of the electronic bands) rather than attributing it to SML.

In summary, we demonstrate that the orbital hybridization between FM and HM layers at the interface can lead to two effects which need to be avoided for efficient spin injection: (1) reduced spin polarization of the FM and (2) enhanced spin relaxation. We show that an MgO interlayer with a thickness of 2 Å leads to optimum results for the spin injection at Ta/CoFeB interfaces. We believe that chemical control of the interface hybridization at the atomic scale (e.g., by ultrathin oxide layers) as demonstrated here is a promising approach to tune and enhance the interface spin transmission and thereby improve the efficiency of many spintronic devices.

■ ASSOCIATED CONTENT

ⓢ Supporting Information

The Supporting Information is available free of charge at https://pubs.acs.org/doi/10.1021/acs.nanolett.1c04358.

> It includes methods for sample preparation and characterization details, transport calculation details, magnetic moment reduction, and extra supporting calculations (PDF)

■ AUTHOR INFORMATION

Corresponding Authors

Mohamed Amine Wahada − *Max Planck Institute for Microstructure Physics, 06120 Halle, Germany;*
Email: awahada@mpi-halle.mpg.de

Georg Woltersdorf − *Institute of Physics, Martin Luther University Halle-Wittenberg, 06120 Halle, Germany; Max Planck Institute for Microstructure Physics, 06120 Halle, Germany;* ⓘ orcid.org/0000-0001-9299-8880;
Email: georg.woltersdorf@physik.uni-halle.de

Authors

Ersoy Şaşıoğlu − *Institute of Physics, Martin Luther University Halle-Wittenberg, 06120 Halle, Germany;* ⓘ orcid.org/0000-0002-1701-528X

Wolfgang Hoppe − *Institute of Physics, Martin Luther University Halle-Wittenberg, 06120 Halle, Germany*

Xilin Zhou − *Max Planck Institute for Microstructure Physics, 06120 Halle, Germany;* ⓘ orcid.org/0000-0003-4135-5070

Hakan Deniz − *Max Planck Institute for Microstructure Physics, 06120 Halle, Germany*

Reza Rouzegar − *Department of Physics, Freie Universität Berlin, 14195 Berlin, Germany*

Tobias Kampfrath − *Department of Physics, Freie Universität Berlin, 14195 Berlin, Germany*

Ingrid Mertig − *Institute of Physics, Martin Luther University Halle-Wittenberg, 06120 Halle, Germany*

Stuart S. P. Parkin − *Max Planck Institute for Microstructure Physics, 06120 Halle, Germany;* ⓘ orcid.org/0000-0003-4702-6139

Complete contact information is available at:
https://pubs.acs.org/10.1021/acs.nanolett.1c04358

Author Contributions

G.W. and S.S.P.P. conceived the project. M.A.W. carried out the experiments and analyzed the data. E.Ş. and I.M. performed the calculations. W.H. built the experimental setup for the ultrafast spin injection. X.Z. performed the MgO deposition. H.D. performed the transmission electron microscopy. R.R. and T.K. performed free-space THz measurements. G.W. and M.A.W. wrote the manuscript.

Notes

The authors declare no competing financial interest.

■ REFERENCES

(1) Maekawa, S.; Valenzuela, S. O.; Saitoh, E.; Kimura, T. *Spin current*; Oxford University Press, 2017; Vol. 22.

(2) Miron, I. M.; Garello, K.; Gaudin, G.; Zermatten, P.-J.; Costache, M. V.; Auffret, S.; Bandiera, S.; Rodmacq, B.; Schuhl, A.; Gambardella, P. Perpendicular switching of a single ferromagnetic layer induced by in-plane current injection. *Nature* **2011**, *476*, 189−193.

(3) Mihai Miron, I.; Gaudin, G.; Auffret, S.; Rodmacq, B.; Schuhl, A.; Pizzini, S.; Vogel, J.; Gambardella, P. Current-driven spin torque induced by the rashba effect in a ferromagnetic metal layer. *Nat. Mater.* **2010**, *9*, 230−234.

(4) Liu, L.; Pai, C.-F.; Li, Y.; Tseng, H. W.; Ralph, D. C.; Buhrman, R. A. Spin-torque switching with the giant spin hall effect of tantalum. *Science* **2012**, *336*, 555−558.

(5) Liu, L.; Lee, O. J.; Gudmundsen, T. J.; Ralph, D. C.; Buhrman, R. A. Current-induced switching of perpendicularly magnetized magnetic layers using spin torque from the spin hall effect. *Phys. Rev. Lett.* **2012**, *109*, 096602.

(6) Parkin, S. S. P.; Hayashi, M.; Thomas, L. Magnetic domain-wall racetrack memory. *Science* **2008**, *320*, 190−194.

(7) Ryu, K.-S.; Thomas, L.; Yang, S.-H.; Parkin, S. Chiral spin torque at magnetic domain walls. *Nat. Nanotechnol.* **2013**, *8*, 527−533.

(8) Fert, A.; Cros, V.; Sampaio, J. Skyrmions on the track. *Nat. Nanotechnol.* **2013**, *8*, 152−156.

(9) Iwasaki, J.; Mochizuki, M.; Nagaosa, N. Current-induced skyrmion dynamics in constricted geometries. *Nat. Nanotechnol.* **2013**, *8*, 742−747.

(10) Sampaio, J.; Cros, V.; Rohart, S.; Thiaville, A.; Fert, A. Nucleation, stability and current-induced motion of isolated magnetic skyrmions in nanostructures. *Nat. Nanotechnol.* **2013**, *8*, 839−844.

(11) Demidov, V. E.; Urazhdin, S.; Ulrichs, H.; Tiberkevich, V.; Slavin, A.; Baither, D.; Schmitz, G.; Demokritov, S. O. Magnetic nano-oscillator driven by pure spin current. *Nat. Mater.* **2012**, *11*, 1028−1031.

(12) Hoffmann, A. Spin hall effects in metals. *IEEE Trans. Magn.* **2013**, *49*, 5172−5193.

(13) Saitoh, E.; Ueda, M.; Miyajima, H.; Tatara, G. Conversion of spin current into charge current at room temperature: Inverse spin-hall effect. *Appl. Phys. Lett.* **2006**, *88*, 182509.

(14) Sinova, J.; Valenzuela, S. O.; Wunderlich, J.; Back, C. H.; Jungwirth, T. Spin hall effects. *Rev. Mod. Phys.* **2015**, *87*, 1213−1260.

(15) Ando, K.; Takahashi, S.; Ieda, J.; Kajiwara, Y.; Nakayama, H.; Yoshino, T.; Harii, K.; Fujikawa, Y.; Matsuo, M.; Maekawa, S.; Saitoh, E. Inverse spin-hall effect induced by spin pumping in metallic system. *J. Appl. Phys.* **2011**, *109*, 103913.

(16) Kampfrath, T.; Battiato, M.; Maldonado, P.; Eilers, G.; Nötzold, J.; Mährlein, S.; Zbarsky, V.; Freimuth, F.; Mokrousov, Y.; Blügel, S.; Wolf, M.; Radu, I.; Oppeneer, P. M.; Münzenberg, M. Terahertz spin current pulses controlled by magnetic heterostructures. *Nat. Nanotechnol.* **2013**, *8*, 256−260.

(17) Seifert, T.; Jaiswal, S.; Martens, U.; Hannegan, J.; Braun, L.; Maldonado, P.; Freimuth, F.; Kronenberg, A.; Henrizi, J.; Radu, I.; Beaurepaire, E.; Mokrousov, Y.; Oppeneer, P. M.; Jourdan, M.; Jakob, G.; Turchinovich, D.; Hayden, L. M.; Wolf, M.; Münzenberg, M.; Kläui, M.; Kampfrath, T. Efficient metallic spintronic emitters of ultra-broadband terahertz radiation. *Nat. Photonics* **2016**, *10*, 483−488.

(18) Gueckstock, O.; Nadvornik, L.; Gradhand, M.; Seifert, T. S.; Bierhance, G.; Rouzegar, R.; Wolf, M.; Vafaee, M.; Cramer, J.; Syskaki, M. A.; Woltersdorf, G.; Mertig, I.; Jakob, G.; Klaui, M.; Kampfrath, T. Terahertz spin-to-charge conversion by interfacial skew scattering in metallic bilayers. *Adv. Mater.* **2021**, *33*, 2006281.

(19) Hoppe, W.; Weber, J.; Tirpanci, S.; Gueckstock, O.; Kampfrath, T.; Woltersdorf, G. On-chip generation of ultrafast current pulses by nanolayered spintronic terahertz emitters. *ACS Applied Nano Materials* **2021**, *4*, 7454−7460.

(20) Zhang, W.; Han, W.; Jiang, X.; Yang, S.-H.; Parkin, S. Role of transparency of platinum−ferromagnet interfaces in determining the intrinsic magnitude of the spin hall effect. *Nat. Phys.* **2015**, *11*, 496−502.

(21) Xia, K.; Kelly, P. J.; Bauer, G. E. W.; Brataas, A.; Turek, I. Spin torques in ferromagnetic/normal-metal structures. *Phys. Rev. B* **2002**, *65*, 220401.

(22) Gupta, K.; Wesselink, R. J. H.; Liu, R.; Yuan, Z.; Kelly, P. J. Disorder dependence of interface spin memory loss. *Phys. Rev. Lett.* **2020**, *124*, 087702.

(23) Rojas-Sánchez, J.-C.; Reyren, N.; Laczkowski, P.; Savero, W.; Attané, J.-P.; Deranlot, C.; Jamet, M.; George, J.-M.; Vila, L.; Jaffrès, H. Spin pumping and inverse spin hall effect in platinum: The essential role of spin-memory loss at metallic interfaces. *Phys. Rev. Lett.* **2014**, *112*, 106602.

(24) Belashchenko, K. D.; Kovalev, A. A.; van Schilfgaarde, M. Theory of spin loss at metallic interfaces. *Phys. Rev. Lett.* **2016**, *117*, 207204.

(25) Dolui, K.; Nikolic, B. K. Spin-memory loss due to spin-orbit coupling at ferromagnet/heavy-metal interfaces: Ab initio spin-density matrix approach. *Phys. Rev. B* **2017**, *96*, 220403.

(26) Bass, J.; Pratt, W. P Spin-diffusion lengths in metals and alloys, and spin-flipping at metal/metal interfaces: an experimentalist's critical review. *J. Phys.: Condens. Matter* **2007**, *19*, 183201.

(27) Galinon, C.; Tewolde, K.; Loloee, R.; Chiang, W.-C.; Olson, S.; Kurt, H.; Pratt, W. P.; Bass, J.; Xu, P. X.; Xia, Ke; Talanana, M. Pd/ag and pd/au interface specific resistances and interfacial spin flipping. *Appl. Phys. Lett.* **2005**, *86*, 182502.

(28) Zhu, L.; Ralph, D. C.; Buhrman, R. A. Effective spin-mixing conductance of heavy-metal−ferromagnet interfaces. *Phys. Rev. Lett.* **2019**, *123*, 057203.

(29) Zhu, L.; Ralph, D. C.; Buhrman, R. A. Spin-orbit torques in heavy-metal−ferromagnet bilayers with varying strengths of interfacial spin-orbit coupling. *Phys. Rev. Lett.* **2019**, *122*, 077201.

(30) Flores, G. G. B.; Kovalev, A. A.; van Schilfgaarde, M.; Belashchenko, K. D. Generalized magnetoelectronic circuit theory and spin relaxation at interfaces in magnetic multilayers. *Phys. Rev. B* **2020**, *101*, 224405.

(31) Zeng, M.; Chen, B.; Lim, S. T. Interfacial electric field and spin-orbitronic properties of heavy-metal/cofe bilayers. *Appl. Phys. Lett.* **2019**, *114*, 012401.

(32) Wesselink, R. J. H.; Gupta, K.; Yuan, Z.; Kelly, P. J. Calculating spin transport properties from first principles: Spin currents. *Phys. Rev. B* **2019**, *99*, 144409.

(33) Tao, X.; Liu, Q.; Miao, B.; Yu, R.; Feng, Z.; Sun, L.; You, B.; Du, J.; Chen, K.; Zhang, S.; Zhang, L.; Yuan, Z.; Wu, D.; Ding, H. Self-consistent determination of spin hall angle and spin diffusion length in pt and pd: The role of the interface spin loss. *Science Advances* **2018**, *4*, No. eaat1670.

(34) Yu, R.; Miao, B. F.; Sun, L.; Liu, Q.; Du, J.; Omelchenko, P.; Heinrich, B.; Wu, Mingzhong; Ding, H. F. Determination of spin hall angle and spin diffusion length in *β*-phase-dominated tantalum. *Phys. Rev. Materials* **2018**, *2*, 074406.

(35) Chen, K.; Zhang, S. Spin pumping induced electric voltage. *IEEE Magnetics Letters* **2015**, *6*, 1−4.

(36) Chen, K.; Zhang, S. Spin pumping in the presence of spin-orbit coupling. *Phys. Rev. Lett.* **2015**, *114*, 126602.

(37) Zhou, C.; Liu, Y. P.; Wang, Z.; Ma, S. J.; Jia, M. W.; Wu, R. Q.; Zhou, L.; Zhang, W.; Liu, M. K.; Wu, Y. Z.; Qi, J. Broadband terahertz generation via the interface inverse rashba-edelstein effect. *Phys. Rev. Lett.* **2018**, *121*, 086801.

(38) Jungfleisch, M. B.; Zhang, Q.; Zhang, W.; Pearson, J. E.; Schaller, R. D.; Wen, H.; Hoffmann, A. Haidan Wen, and Axel Hoffmann, "Control of terahertz emission by ultrafast spin-charge current conversion at rashba interfaces. *Phys. Rev. Lett.* **2018**, *120*, 207207.

(39) Huisman, T.; Mikhaylovskiy, R.; Costa, J.; Freimuth, F.; Paz, E.; Ventura, J.; Freitas, P. P.; Blügel, S.; Mokrousov, Y.; Rasing, Th.; Kimel, A. V. Femtosecond control of electric currents in metallic ferromagnetic heterostructures. *Nat. Nanotechnol.* **2016**, *11*, 455.

(40) Li, G.; Medapalli, R.; Mikhaylovskiy, R. V.; Spada, F. E.; Rasing, Th.; Fullerton, E. E.; Kimel, A. V. Thz emission from co/pt bilayers with varied roughness, crystal structure, and interface intermixing. *Phys. Rev. Materials* **2019**, *3*, 084415.

(41) Zhang, Q.; Luo, Z.; Li, H.; Yang, Y.; Zhang, X.; Wu, Y. Terahertz emission from anomalous hall effect in a single-layer ferromagnet. *Phys. Rev. Applied* **2019**, *12*, 054027.

(42) Zhu, L.; Ralph, D. C.; Buhrman, R. A. Enhancement of spin transparency by interfacial alloying. *Phys. Rev. B* **2019**, *99*, 180404.

(43) Gueckstock, O.; Nadvornik, L.; Gradhand, M.; Seifert, T. S.; Bierhance, G.; Rouzegar, R.; Wolf, M.; Vafaee, M.; Cramer, J.; Syskaki, M. A.; Woltersdorf, G.; Mertig, I.; Jakob, G.; Klaui, M.; Kampfrath, T. Terahertz spin-to-charge conversion by interfacial skew scattering in metallic bilayers. *Adv. Mater.* **2021**, *33*, 2006281.

(44) Deorani, P.; Yang, H. Role of spin mixing conductance in spin pumping: Enhancement of spin pumping efficiency in ta/cu/py structures. *Appl. Phys. Lett.* **2013**, *103*, 232408.

(45) Lin, W.; Chen, K.; Zhang, S.; Chien, C. L. Enhancement of thermally injected spin current through an antiferromagnetic insulator. *Phys. Rev. Lett.* **2016**, *116*, 186601.

(46) Jin, L.; Jia, K.; Zhang, D.; Liu, B.; Meng, H.; Tang, X.; Zhong, Z.; Zhang, H. Effect of interfacial roughness spin scattering on the spin current transport in yig/nio/pt heterostructures. *ACS Appl. Mater. Interfaces* **2019**, *11*, 35458−35467.

(47) Parkin, S. S. P. Dramatic enhancement of interlayer exchange coupling and giant magnetoresistance in ni81fe19/cu multilayers by addition of thin co interface layers. *Appl. Phys. Lett.* **1992**, *61*, 1358−1360.

(48) Parkin, S. S. P. Origin of enhanced magnetoresistance of magnetic multilayers: Spin-dependent scattering from magnetic interface states. *Phys. Rev. Lett.* **1993**, *71*, 1641−1644.

(49) Guan, Y.; Zhou, X.; Ma, T.; Blasing, R.; Deniz, H.; Yang, S.-H.; Parkin, S. S. P. Increased Efficiency of Current-Induced Motion of Chiral Domain Walls by Interface Engineering. *Adv. Mater.* **2021**, *33*, 2007991.

(50) Miura, Y.; Tsujikawa, M.; Shirai, M. A first-principles study on magnetocrystalline anisotropy at interfaces of fe with non-magnetic metals. *J. Appl. Phys.* **2013**, *113*, 233908.

(51) Kowalewski, M.; Butler, W. H.; Moghadam, N.; Stocks, G. M.; Schulthess, T. C.; Song, K. J.; Thompson, J. R.; Arrott, A. S.; Zhu, T.; Drewes, J.; Katti, R. R.; McClure, M. T.; Escorcia, O. The effect of ta on the magnetic thickness of permalloy (ni$_8$fe$_1$9) films. *J. Appl. Phys.* **2000**, *87*, 5732−5734.

(52) Tserkovnyak, Y.; Brataas, A.; Bauer, G. E. W. Enhanced gilbert damping in thin ferromagnetic films. *Phys. Rev. Lett.* **2002**, *88*, 117601.

(53) Rouzegar, R.; Brandt, L.; Nadvornik, L.; Reiss, D. A.; Chekhov, A. L.; Gueckstock, O.; In, C.; Wolf, M.; Seifert, T. S.; Brouwer, P. W.; Woltersdorf, G.; Kampfrath, T. *Laser-induced terahertz spin transport in magnetic nanostructures arises from the same force as ultrafast demagnetization*; arXiv:2103.11710 [cond-mat.mes-hall] (2021), https://arxiv.org/abs/2103.11710 (last accessed 25.02.2022).

(54) Herapath, R. I.; Hornett, S. M.; Seifert, T. S.; Jakob, G.; Kläui, M.; Bertolotti, J.; Kampfrath, T.; Hendry, E. Impact of pump wavelength on terahertz emission of a cavity-enhanced spintronic trilayer. *Appl. Phys. Lett.* **2019**, *114*, 041107.

(55) Sinha, J.; Hayashi, M.; Kellock, A. J.; Fukami, S.; Yamanouchi, M.; Sato, H.; Ikeda, S.; Mitani, S.; Yang, S.-h.; Parkin, S. S. P.; Ohno, H. Seiji Mitani, See-hun Yang, Stuart S. P. Parkin, and Hideo Ohno, "Enhanced interface perpendicular magnetic anisotropy in ta− cofeb− mgo using nitrogen doped ta underlayers. *Appl. Phys. Lett.* **2013**, *102*, 242405.

(56) Cuchet, L.; Rodmacq, B.; Auffret, S.; Sousa, R. C.; Dieny, B. Influence of magnetic electrodes thicknesses on the transport properties of magnetic tunnel junctions with perpendicular anisotropy. *Appl. Phys. Lett.* **2014**, *105*, 052408.

(57) Sato, N.; O'Brien, K. P.; Millard, K.; Doyle, B.; Oguz, K. Investigation of extrinsic damping caused by magnetic dead layer in ta-cofeb-mgo multilayers with perpendicular anisotropy. *J. Appl. Phys.* **2016**, *119*, 093902.

(58) Shen, S.-H.; Lee, D.-S.; Cheng, C.-W.; Chan, W.-J.; Chern, G. The correlation between magnetic dead layer and perpendicular magnetic anisotropy in mgo/cofeb/ta top structure. *IEEE Trans. Magn.* **2019**, *55*, 1−5.

(59) Urban, R.; Woltersdorf, G.; Heinrich, B. Gilbert damping in single and multilayer ultrathin films: Role of interfaces in nonlocal spin dynamics. *Phys. Rev. Lett.* **2001**, *87*, 217204.